ELSEVIER

Journal of Structural Geology 29 (2007) 1267–1280

JOURNAL OF STRUCTURAL GEOLOGY

www.elsevier.com/locate/jsg

Inference of trishear-faulting processes from deformed pregrowth and growth strata

M.L. Lin [a], C.P. Wang [b], W.S. Chen [c], C.N. Yang [c], F.S. Jeng [a,*]

[a] *Department of Civil Engineering, National Taiwan University, Taipei, Taiwan*
[b] *Department of Geotechnical Engineering, CECI Engineering Consultants, Inc., Taipei, Taiwan*
[c] *Department of Geosciences, National Taiwan University, Taipei, Taiwan*

Received 7 December 2004; received in revised form 9 March 2007; accepted 23 March 2007
Available online 14 April 2007

Abstract

Near surface strata deformed by propagation of a fault situated underneath these strata hold explicit records of fault activities. The delicate deformed strata exposed in investigation trenches for paleoseismologic study conform to fault-propagation folds growing above a blind thrust. Growth strata deposited subsequently across the coseismic fold scarps are preserved by onlap and unconformities. Information from these sedimentary and folding processes was used in conjunction with inverse modeling using the trishear model technique proposed by Allmendinger (Allmendinger, R.W., 1998. Inverse and forward numerical modeling of trishear fault-propagation folds. Tectonics 17, 640–656) in estimating the times and amounts of slips. This methodology becomes necessary especially when the extent of a deformed profile is insufficiently exposed to observation or the location of the fault tip is invisible. The proposed method can deal with growth strata that can be selectively removed during fold restoration.

The interpretations on the deformation history obtained by inverse analysis and trench investigation were then compared. The combination of these two approaches seemed to enhance and complement each other and allows a better and more complete understanding of the trishear-faulting processes and is useful in seismic hazard assessment.

Keywords: Trishear; Fault; Inverse analysis; Faulting processes; Onlap deposits; Chichi earthquake; Chelungpu Fault; Paleoseismology

1. Introduction

1.1. Background

Near ground surface geologic strata are readily deformed and folded by up-thrust movements of an underlying blind fault induced by major earthquake. These strata may have been uplifted many times by intermittently recurring major earthquakes over the long span of the geologic past. The geometry of such near surface strata hence holds explicit records of past fault movements. With appropriate techniques these records should yield information on fault frequency as well as how the fault accumulated slip during previous major earthquakes.

The studied fault, the Chelungpu Fault, was re-activated during the 1999 Chichi earthquake event (Chen et al., 2001a). Investigation trenches were excavated to examine the deformed surficial strata that contain records of past fault movements. The profile of delicate deformed strata with several times of fault movements obtained from a trench located in Nantou County was selected for paleoseismological study (Fig. 1). As a result, three seismic events were identified, which are named as *E2*, *E1* and the Chichi events in their sequence of occurrence (Chen et al., 2007a).

The monoclinal morphological features of ground surface and bedding, downward steepening of forelimb strata and smoothly rounded fold-hinges exposed in this trench are consistent with a trishear fault-propagation fold growing above

* Correspondence to: Department of Civil Engineering, National Taiwan University, No. 1, Sec. 4, Roosevelt Road, 10617 Taipei, Taiwan. Tel./fax: +886 2 2364 5734.
E-mail address: fsjeng@ntu.edu.tw (F.S. Jeng).

0191-8141/$ - see front matter © 2007 Published by Elsevier Ltd.
doi:10.1016/j.jsg.2007.03.017

Fig. 1. Appearances of northern wall of the studied trench. The photo has been flipped horizontally for comparison with the inversion results. The trench has a length of 27 m and a depth of 7 m, which comprises 3 stages with a height of about 2 m for each stage. The monoclinal morphological features of ground surface and beddings, downward steepening of forelimb strata, and smoothly rounded fold-hinges are consistent with a trishear fault-propagation fold growing above a blind thrust.

a blind thrust. Several exposed pregrowth strata indicate explicitly that the blind thrust slipped more than once and total amount of the slip is greater than the slip of the latest Chichi event. Because the fault tip was not exposed in the trench, many issues about fault propagation are ambiguous. For example, the locations of the fault tips and the ramp angle of the blind thrust are hard to figure out. As a result, the times of fault movement, the amounts of fault slip for each of the previous major earthquake events, and the accommodation of deformation within the trishear zones pose questions. The answers to these questions would be useful in seismic hazard assessment of blind fault propagation, especially in urban area with thick soft sedimentary cover.

Digitized layers of surfical strata are analyzed through inverse modeling to understand the trishear fault-propagation fold growing processes. Growth strata deposited subsequently across the coseismic fold scarps are preserved by onlap and unconformities on the monoclinal surface. This information enables an additional test on the validity of the proposed procedures for the repeating alternation of fault slipping and sediment deposition.

Fault-propagation folding in homogeneous strata usually creates monoclinal morphological features of ground surface and bedding, smoothly rounded fold-hinges in front of propagating blind thrust, downward steepening of forelimb strata towards the fault tips and ductile deformation within folded strata. Trishear fault-propagation folding model provides an important alternative to a progressive kink folding model for characterizing these features (Allmendinger, 1998; Erslev, 1991; Ford et al., 1997; Hardy and Ford, 1997; Hardy and McClay, 1999; Suppe and Medwedeff, 1990; Zehnder and Allmendinger, 2000). With increasing clarification of the trishear fault, seismic hazard assessment on faults with propagation approaching the ground surface becomes possible (Allmendinger and Shaw, 2000; Champion et al., 2001; Lin et al., 2006).

The velocity fields and the determination of associated parameters of the trishear model have been proposed (Allmendinger and Shaw, 2000; Cardozo, 2005; Zehnder and Allmendinger, 2000), compared to an experimental study (Withjack et al., 1990) and extended to simulate 3-dimentional folding (Cristallini and Allmendinger, 2001). Strata may grow and also deform in intervals between major earthquakes, the phenomenon should hence also be taken into consideration in subsequent deformation (Ford et al., 1997; Hardy and Ford, 1997; Hardy and McClay, 1999).

While the trishear kinematic model seems to explain well the geometric development and finite strain of triangular fault-propagation folds, there have been few applications to coseismic deformation induced by blind faults propagating upwards into the cover of soft sediments (e.g. Allmendinger, 1998; Allmendinger and Shaw, 2000; Erslev, 1991; Hardy and Ford, 1997; Hardy and McClay, 1999; Zehnder and Allmendinger, 2000).

In this study, a program was developed to perform inverse modeling. This program produced results similar to those obtained through the program developed by Zehnder and Allmendinger (2000) for trishear modeling of fault slip. The adopted inverse method, also based on the ideas of Allmendinger (1998) is characterized by: (1) the use of the growth strata in identifying the major events, which can be selectively removed during the inverse analysis; and (2) the use of more than one layer as key beds to control the search of best-fit parameters. The number of major earthquake events and the corresponding deformations can accordingly be estimated.

If a blind fault had experienced multiple slip events, strata near the fault tip would be more severely folded than strata near the ground surface. The extent of the triangular trishear zone decrease while the tip approaches the ground surface. The present study allows restoring several deformed strata, either severely folded or only gently bent, into their original straight settings.

The geological significances of these inferred paleoseismologic trishear-faulting processes from deformed pregrowth and growth strata are: (1) the amounts of slips can possibly reflect the magnitude of the paleo-earthquakes; (2) the sedimentary environment for growth strata might be inferred from the initial dip angles of restored strata; and (3) the major fault planes and fault tips of these paleoseismologic events can be inferred.

1.2. Basics of trishear faulting

Assuming no change in area during fault propagation folding, the components of the velocity field can be expressed as (Fig. 2a; modified after Zehnder and Allmendinger, 2000):

$$V_x = \frac{V_0}{2}\left[\left(\frac{y}{x \cdot \tan\phi}\right) + 1\right] \tag{1}$$

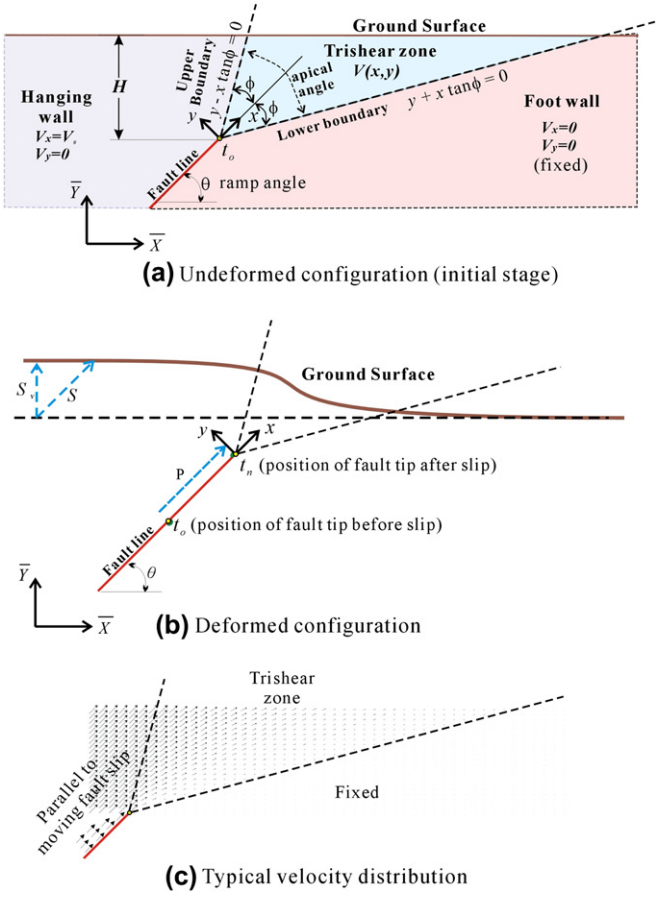

Fig. 2. Configuration of the trishear zone and corresponding definitions. Part (a) shows the definitions of the ramp angle (θ), apical angle (2φ), the vertical distance from the ground surface to the fault tip (H), the boundaries of deformation and coordinates before deformation. Part (b) shows the deformed configuration, the definition of fault slip (also the ground movement of up-thrown block) S, vertical uplift (S_v) and fault tip propagation P. Part (c) shows a typical velocity distribution within the strata during trishear deformation. The strata on hanging wall side are significantly displaced and the strata on the footwall side remain fixed. As a result, the strata between the two zones are severely distorted.

$$V_y = \frac{V_0}{4}\left[\left(\frac{y^2}{x^2 \cdot \tan\phi}\right) - \tan\phi\right] \tag{2}$$

where ϕ is half of the apical angle of trishear zone based on the assumed symmetric trishear zone; V_0 is velocity of the fault slip; and V_x and V_y are the velocity components along the x- and y-direction, respectively. A typical distribution of velocity is depicted by the vectors in Fig. 2c. During the fault propagation (Fig. 2a,b), the fault slips a distance S and the fault tip (t_o, and the vertical distance from the ground surface to the fault tip is marked H) propagates a distance P along the fault line, in which P can be either equal to or greater than S. The newly developed fault line, from its initial position t_o to its current position (marked t_n), has a ramp angle of θ. The ground surface movement of the hanging wall (away from the trishear deformation zone) is indicated as S, and the uplift (the vertical component of S) of the ground surface along the hanging wall side is indicated as S_v (Fig. 2b). It is found that S is often smaller than the fault slip P and is controlled by the propagation to slip ratio (P/S) (Champion et al., 2001). The material located within the footwall, which is alongside the trishear zone, remains fixed. During the faulting process, the trishear zone is always bounded by an upper boundary and a lower boundary (Fig. 2a). As illustrated by Fig. 2b, in addition to ϕ, the geometry of the deformed strata is also determined by θ, H, S, P, P/S, and locations of the fault tips (t_o and t_n). The ground uplift S_v can be related to S and θ as: $S_v = S \sin\theta$. Detailed definitions, boundary conditions and interpretations of the trishear zone can be seen in Allmendinger (1998) and Zehnder and Allmendinger (2000).

2. Methodology

2.1. Criteria for key layers

The kinematic trishear model well relates fold geometry to fault ramp and slip in homogeneous, isotropic materials as validated in mechanic modeling (Cardozo et al., 2003; Cardozo, 2005; Johnson and Johnson, 2002). Because the soft sediments found in the trench for paleoseismologic analysis are relatively young and not compacted, these strata may behave as relatively homogeneous, isotropic materials. This may account for the good fit between trench result and trishear modeling. In trench sites, soft sediments may comprise varied types of soils, including sandy soil, clayey soil or gravels (Chen et al., 2004, 2007a). Only the clayey soils may serve as good key layers used for digitization in modeling because their bedding boundaries are relatively distinct.

2.2. Analyzing program

In this study, a program was developed first to simulate forward and inverse trishear deformation. The algorithm relies on a backward modeling approach as described by Allmendinger (1998, 2005). One can restore layers backward to their unfolded original planar configurations. When the set

of parameters and the initial location of fault tip are unknown, searching for the parameters that best fit the deformed strata becomes necessary, since these parameters can not be identified by simply observing the deformed strata. Indeed, the search for the best fit parameters is the most essential component required for the inverse analysis. The statistic index used to evaluate goodness of fitting is the root mean square of total differences in distances between idealized initial inclined planar layers and the restored layers. The root mean squares of total differences corresponding to several selected key layers are summed and serve as the criterion in judging whether the search is acceptable. The set of parameters leading to a minimum value serves as the most representative set.

It was found that the results produced by the developed program were identical to the results produced by the program freely provided by Allmendinger (2005). This indicates that both the original program and the later developed program produce comparable results.

2.3. Inverse analysis

To simplify, parameters such as the ramp angle, apical angle and *P*/*S* ratio of trishear model are assumed to remain invariable during all of fault propagation events.

Exposed near the trench bottom, the severely folded pregrowth strata are firstly restored into their supposed straight strata to seek the best fit parameters (t_o, t_n, θ, ϕ, S and P/S). The inclinations of these straight strata are defined as initial dip angles of these strata (α).

The parameters, such as ramp angle, apical angle, *P*/*S* ratio and locations of fault tips of previous events of underlying pregrowth strata are obtained and serve as known parameters. Growth strata that experienced less fault propagation events than the underlying pregrowth strata are then analyzed following the same procedures. Each one of the overlying growth strata with various slips is restored to their supposed straight stratum. Therefore, we can infer the corresponding fault tips ($t_{n\text{-}1}$, $t_{n\text{-}2}$ …) and fault slips for each one of the growth strata. Subsequently, successive growth strata with similar total slips in a sequence are sorted into each such group of strata representing a sedimentary sequence bounded by two fault slip events. The numbers of events and amounts of slips of fault movements may possibly reflect the numbers and magnitude of the corresponding paleo-earthquakes.

3. Background of the studied fault

3.1. Chelungpu Fault and trench site

The Chelungpu Fault is one of the major thrust faults within the Western Foothill region in west-central Taiwan. The fault was re-activated during the 1999 Chichi earthquake event. The Chichi earthquake had a magnitude (M_W) of 7.6 and epicenter in west-central Taiwan with a rather shallow depth of about 8 km. The resultant surface trace exceeded 100 km in length and hanging wall uplifts ranged from 2 to 10 m (Fig. 3, modified from Chen et al., 2001a). This severe earthquake caused a death toll of 2500 persons and significant loss of property in Taiwan.

Investigation trenches were excavated at nine sites along the fault trace. The purposes of trenching were: (1) to unravel the number of previous major earthquake events; (2) to acquire suitable material for dating the time when these major events occurred; and (3) to observe deformation associated with these past events (including the Chichi earthquake) (Chen et al., 2001a,b,c,d 2004, 2007a,b; Lee et al., 2001, 2004). Detailed information on these trenches can be found as the follows (Fig. 3): the Fengyuan site (Ota et al., 2005), the Wenshanfarm site (not published yet), the Pineapple-field site (Chen et al., 2004), the Siangong-temple site (Chen et al., 2004), the Wanfung site (Chen et al., 2001b), the Tsaotun site (Ota et al., 2001), the Shijia site (Chen et al., 2004; this study), the Mingjian site (Chen et al., 2001c), and the Chushan site (Chen et al., 2007b).

At Siangong temple site and Shijia site, the fault tips were not exposed (Chen et al., 2007a). The Shijia site located at Bauwei in Nantou County in west-central Taiwan was selected as the studied site (Figs. 5–7). The accumulated slips of underlying blind Chelungpu Fault at Shijia site were very significant so that its hanging wall formed hills, which exhibited a strong morphological contrast on the two sides of the fault trace (Fig. 4). On the footwall of the Chelungpu Fault, the ground surface has a gently westward dipping slope of approximately 3° (Chen et al., 2007a).

The studied trench at Shijia site was excavated normal to the fault line, the trend of which is N10°W. A stretch of at least 300 m of this rupture line runs perpendicular to the two sides of the trench, thus it is reasonable to consider the deformation is approximately 2-dimensional for this trench.

There were two trenches excavated at Shijia site. In 2000 Trench 1 (adjacent trench) was excavated for investigation. The ‘‘adjacent’’ trench had a length of 33 m and a depth of 6 m. This trench was abandoned due to collapse of the walls. A new trench, Trench 2 (studied trench) was opened in 2001 at a site immediately north of Trench 1. For better observation on key beds for inverse modeling, Trench 2 was located closer to the central part of the monocline fold profile.

3.2. Interpreted strata and boreholes

The trench had a length of 27 m and a depth of 7 m, comprised 3 stages with a height of about 2 m for each stage (Figs. 1 and 5). There were 21 soil layers exposed in the trench, marked as *Layer u* to *Layer a* from the bottom of trench to the ground surface (Fig. 5).

Detailed description on paleoseismologic and sedimentary characteristics for these layers are presented by Chen et al. (2007a). A summary is as follows: Shallow subsurface deposits predominantly consist of well-sorted fine sand interbedded with mud and humic paleosoil, which represent overbank deposits. Trench wall exposures show three depositional units (cw1, cw2 and cw3) defined by onlapped surface of humic paleosoil horizons (H1 and H2, Fig. 5). The lower sequence of unit cw3 consists of 5-m-thick alternately thick-bedded silt with thin-bedded mud

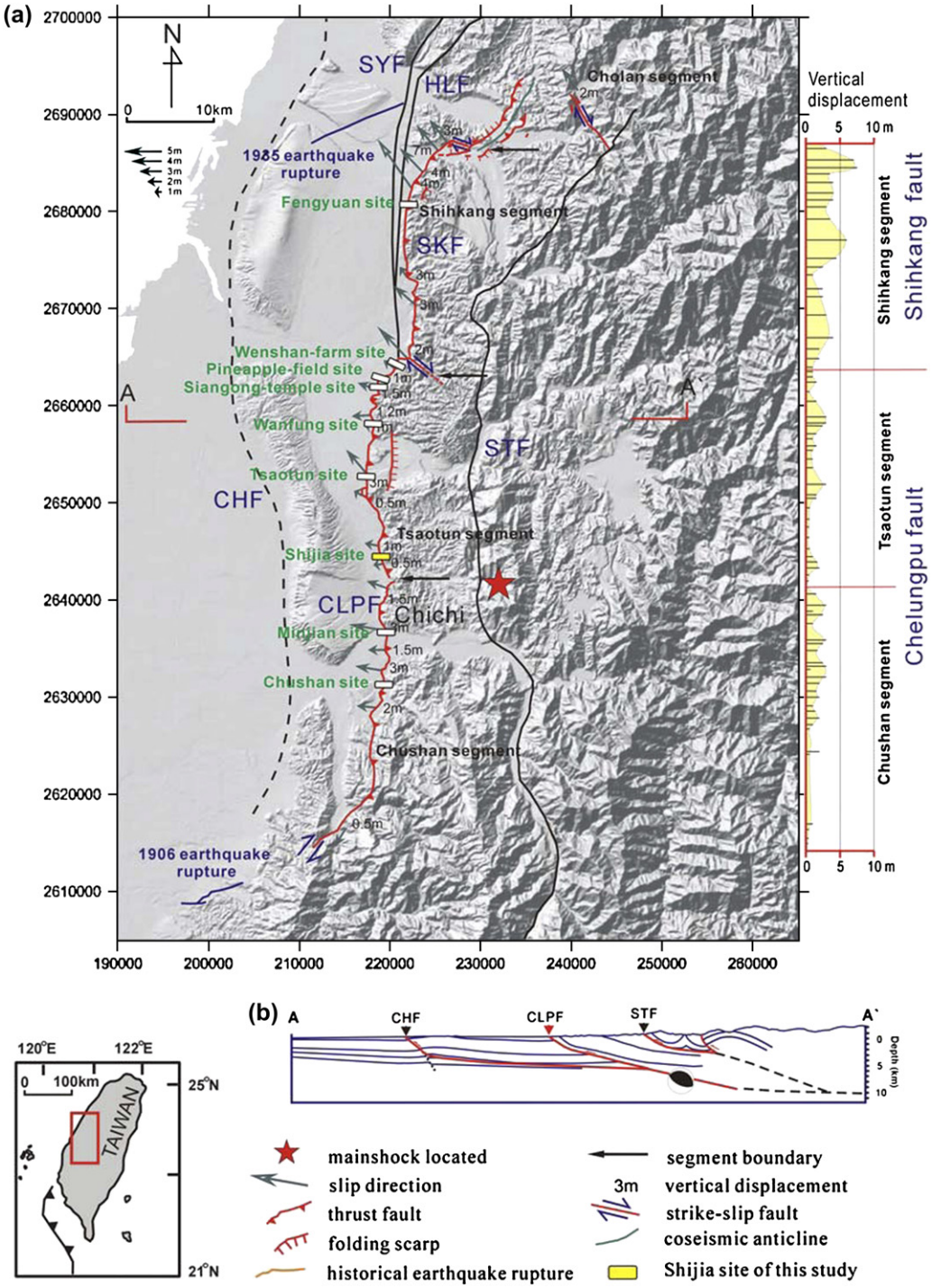

Fig. 3. Geological setting, locations of the trench sites, the distribution and the uplift magnitudes of the Chelungpu Fault (CLPF) in west-central Taiwan (modified after Chen et al., 2001a). (a) The Chichi earthquake causes a surface rupture in front of the Western Foothills. The surface rupture is subdivided into four segments: the Chushan, Tsaotun, Shihkang, and Cholan segments along the Chelungpu Fault. Slip vectors and vertical displacements of fault rupture and fold scarps are indicated in three N-S trending segments: (1) Shihkang segment along the Shihkang fault, which has a N30–40°W displacement with a length of 2–7 m; (2) Tsaotun segment along the Chelungpu fault, which has a N70–90°W displacement with a length of 0.5–3 m; and (3) Chushan segment along the Chelungpu fault, which has a N80–90°W displacement with a length of 0.5–3 m. CHF: Changhuang fault, CLPF: Chelungpu fault, HLF: Houli fault, SKF: Shihkang fault, STF: Shuangtung fault, SYF: Sanyi fault, TJSF: Tajianshan fault; (b) The seismic reflection profiles are re-projected onto the cross section A-A′ (after Hung and Wiltschko, 1993; Chen et al., 2001a).

and humic paleosoil horizons (Fig. 5). The upper sequence shows two wedge-shaped alluvial deposits of units cw1 and cw2 which are exposed at the footwall of monoclinal fold in the trench wall exposures. The two units onlapped H1 and H2 humic paleosoils on the forelimb, respectively. The onlapped relation indicates a folding after deposition of the H1 and H2 paleosoils.

Deposition of onlap deposits after ancient earthquake events enables an additional test on the validity of the

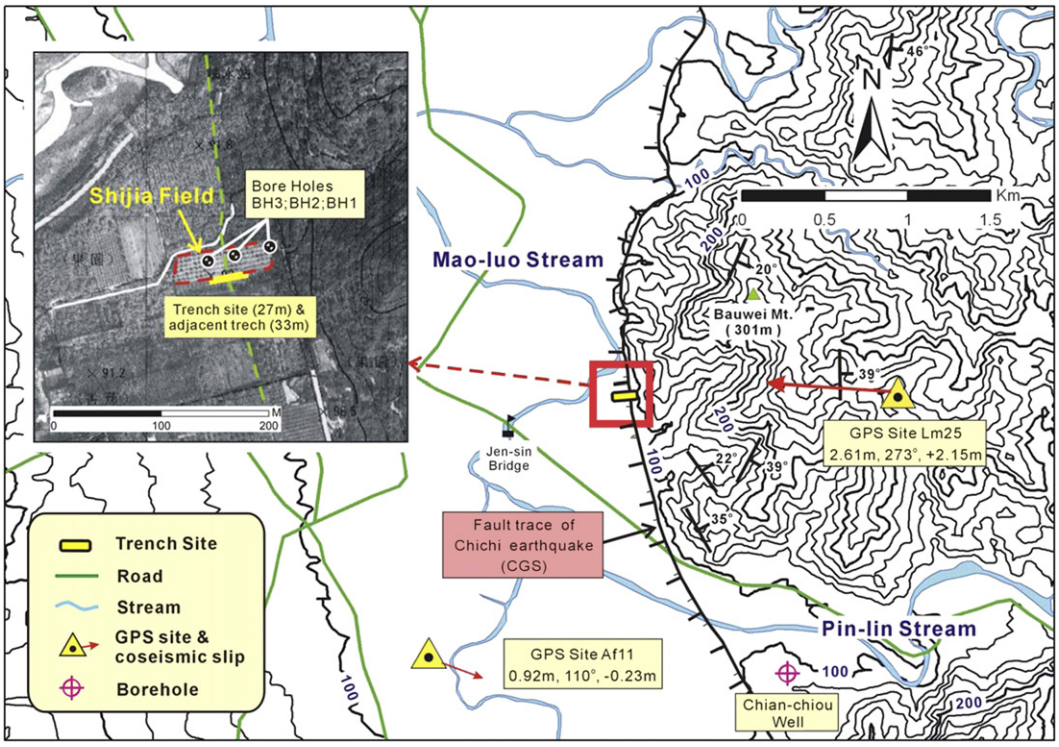

Fig. 4. Locations of the Shijia trench site, fault line and co-seismic ground movements measured by GPS devices at Bauwei (Lm 25) in Nantou County in west-central Taiwan. The solid line with tick marks indicates the downthrown side of the Chelungpu fault reactivated by Chichi earthquake (after Central Geological Survey, 2000). The east side of the scarp was lifted up 2 ~ 3 m relative to the west side during Chichi earthquake. Locations of Shija trenches and boreholes are shown in the insert.

proposed procedures for inference of trishear-faulting processes from deformed pregrowth and growth strata.

The fold geometries of the studied trench and the adjacent trench are depicted in Fig. 5. The strata had been substantially deformed by events before the Chichi earthquakes and also by the Chichi earthquake (Figs. 1 and 5). The exposed deformation pattern is conformable to that of the trishear model.

The deformation patterns of the strata are similar in both trenches. The only difference lies in that the ground surface layer of Trench 2 was slightly disturbed during excavation of Trench 1. However, the intact and un-disturbed top layer boundary of the Trench 1 was preserved. Therefore, it seemed reasonable to assume that the configuration of the top layer of Trench 2 is also un-disturbed, the same as that of Trench 1 (Fig. 5b).

On top of the pre-growth strata there are growth strata. Wedges of the growth strata terminate around the fold scarp, implying that they are growth strata formed consequently to coseismic folding (Fig. 5).

Three boreholes (BH1, BH2, and BH3) were sunk revealing the underground strata near the studied trench (Figs. 4 and 6, Chen et al., 2007a). The contacts between older Chinshui Formation and younger gravel beds indicate the probable fault surfaces; these allowed recognition of three probable locations of the fault planes with corresponding probable ramp angles of 25° ~ 35° or 45° ~ 50° (Fig. 6, Chen et al., 2007a).

Information from borehole logging indicated the possible locations of the blind fault, and also showed that the thickness of overburden in the studied sites is about 10 m. This thickness seems to prevent fault rupturing from surfacing on the ground.

4. Inference of past trishear faulting processes

Eleven readily recognizable sand and clay layer boundaries were recorded, and they were designated *Boundaries #1 ~ #11*. Subsequently, marker-points along each selected layer boundary were digitized (Fig. 7). Bounded by *Boundaries #1 ~ #5*, ten growth strata layers were identified. Beneath *Boundary #5*, eight pre-growth layers (bounded by *Boundaries #5–#11*) were identified (Fig. 7).

The eight pre-growth layers (*Layer m* to *Layer t* from the topmost layer to the lowest layer) have fairly uniform thickness outside the trishear deformation zone. Among these eight layers, only the top two layers (*Layer m* and *Layer n*) were exposed over the hanging and the foot wall, while the lower layers were not exposed in the footwall within the trench (Figs. 5 and 7). The amount of the total uplift estimated from the pregrowth strata is 3.7 m, which is larger than the 2.51 m uplift induced by Chichi event. The deformation of these pregrowth strata then yielded records of a number of fault movements. Since these eight layers are uniform in thickness, it is difficult to differentiate whether the current deformations was induced by one or more fault slips through the method proposed by Chen et al. (2007a).

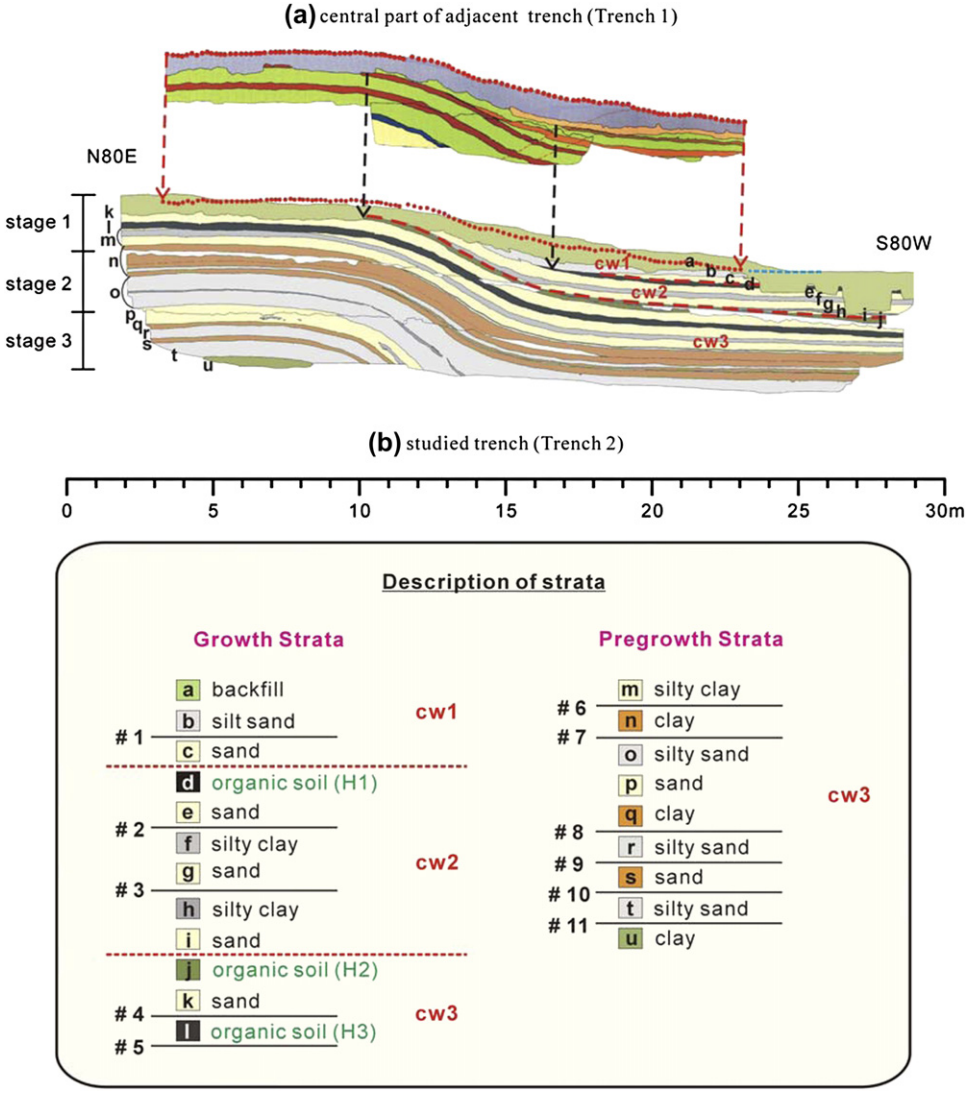

Fig. 5. Interpretation of north wall strata of the: (a) Adjacent trench (Trench 1) south to the studied trench, which has an un-disturbed top soil stratum; and (b) The studied trench (Trench 2). Marker-points line represents the assumed undisturbed ground surface.

Based on the configuration of the existing deformation, the search ranges and the increments of parameters are selected as (Fig. 7): $\theta = 25^\circ \sim 45^\circ$; $\Delta\theta = 5^\circ$; $\varphi = 5^\circ \sim 55^\circ$; $\Delta\varphi = 5^\circ$; $P/S = 0.5 \sim 4$; $\Delta(P/S) = 0.5$; $x = 7 \sim 15$ m; $\Delta x = 0.5$ m; $y = -4 \sim 3$ m; $\Delta y = 0.5$ m; $S = 6 \sim 7$ m; and $\Delta S = 0.01$. Restoration of current boundaries (*#5 ~ #11*) of the pregrowth strata into straight lines was firstly conducted to evaluate the corresponding parameters, θ, φ, P/S ratio, t_o, t_c, α and S. Remarkably, the estimated S is the accumulated slips of all events. Subsequently, how far each one of the growth strata slipped was deduced through the restoration of the deformed growth strata. The discontinuous slips from t_o to t_c as well as the events triggering the fault tip propagation may be further identified.

4.1. Coseismic faulting history revealed by inverse analyses

Inverse modeling indicates that the best fit ramp angle, apical angle and *P/S* ratio and total slip of the pregrowth strata are 35°, 80°, 2.5 and 6.45 m, respectively. The results of inverse analyses reveal that there were three coseismic slips of corresponding earthquake events, *EQ2*, *EQ1* and the Chichi earthquake in the order of occurrences. The estimated amounts of the slips for each event were 0.14, 1.94 and 4.37 m, respectively. The estimated slip and corresponding parameters of trishear deformation for these three events are summarized in Table 1. The summaries of statistics for best fitting parameters of the pregrowth strata are shown in Fig. 8. The processes of the three coseismic slips are depicted in Fig. 9. For the sake of convenience, they are described in forward sequence as follows:

(1) before the occurrence of *EQ2*, the fault tip is located at t_o (Fig. 9a). The *Boundary #5* was the ground surface before *EQ2*. *Boundaries #5–#11* were straight lines with a dip angle of 0.43°;
(2) the occurrence of *EQ2* caused a 0.35 m propagation of fault tip and moved it to t_A (Fig. 9b). The fault slip was 0.14 m. Afterward, several growth strata (bounded by

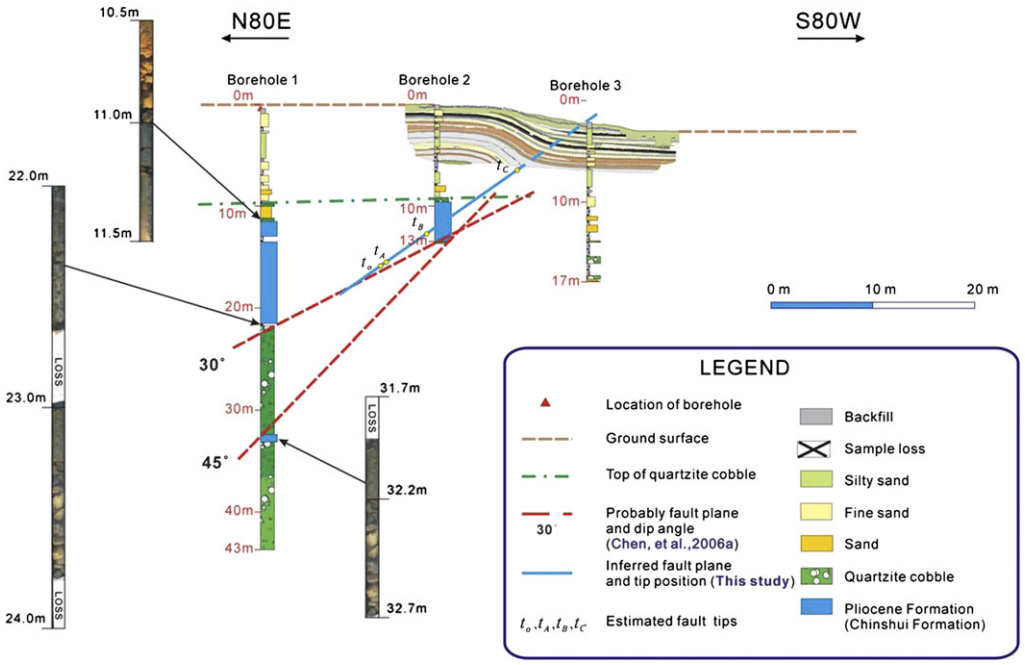

Fig. 6. Possible locations and orientations of CLPF revealed by boreholes. The locations of the boreholes are shown in Fig. 4. BH1 indicate the contacts between the older Pliocene Chinshui Formation and the much younger gravel layers at depth 31.7 ~ 32.7 m, 22.0 ~ 24.0 m, and the contact between soft sediment cover and the Chinshui Formation at depth 10.5 ~ 11.5 m.

Boundaries #5 and #3) were deposited (Fig. 9c). *Boundaries #4* and *#3* were straight lines with a dip angle of 0.63°. There is a wedge deposit beneath *Boundary #4*;

(3) the occurrence of *EQ1* caused a 4.85 m propagation of fault tip and moved it to t_B (Fig. 9d). The fault slip was 1.94 m. Afterward, several growth strata (bounded by *Boundaries* #3 and the current ground surface) were deposited (Fig. 9e). *Boundaries #2* and *#1* were straight lines with a dip angle of 0.29°. There are wedge deposits underneath *Boundaries #1* and *#2*, respectively; and

(4) the occurrence of Chichi earthquake resulted in a 10.93 m propagation of the fault tip and moved it to t_C (Fig. 9f). The fault slip was 4.37 m and the ground uplift (S_v) was 2.51 m by the Chichi event (Table 1).

Fig. 10 summarizes the propagations of the fault tips, inferred from the proposed inverse analysis. The fault tip was located at t_o before *Earthquake EQ2* occurred, and moved to t_a, t_b and t_c respectively, consequent to occurrences of *EQ2*, *EQ1* and the Chichi events.

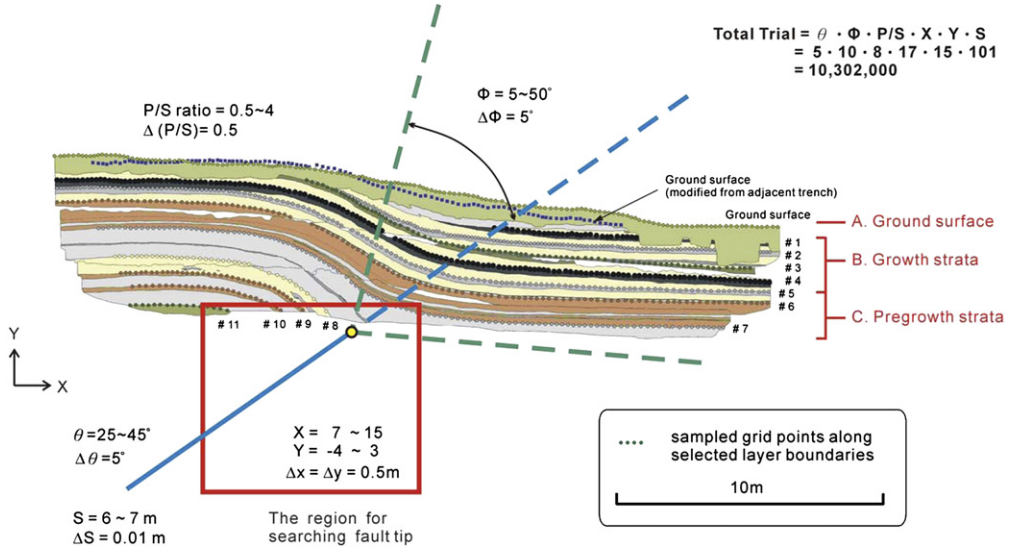

Fig. 7. Interpretation of strata exposed by trench excavation and the ranges of parameters selected for inverse analysis. The step sizes for parameters are indicated in the figure. The total number of trials is 10,302,000. The origin of the x and y coordinates is also shown in the figure.

Table 1
Best-fit parameters found by inverse analyses

Stage	Key bed	Best-fit parameters						
		Location of fault tip (m)	S (m)	S_v (m)	P/S	θ	φ	α
After Chichi	Ground surface, *Boundaries #1, #2* (growth strata)	t_C (12.5, 2.0)	4.37	2.51	2.5	35°	40°	–
After *EQ1*	*Boundaries #3, #4* (growth strata)	t_B (3.6, −4.3)	1.94	1.11	2.5	35°	40°	0.29°
After *EQ2*	*Boundaries #5 ~ #11* (pregrowth strata)	t_A (−0.4, −7.1)	0.14	0.08	2.5	35°	40°	0.63°
Before *EQ2*	–	t_o (−0.7, −7.3)	–	–	–	–	–	0.43°

Remarks: (1) Definitions of the parameters are illustrated in Fig. 1. (2) Locations of the fault tips are shown in Figs. 9 and 10. The origin is shown in Fig. 7. (3) α is the dip angle of the key beds before coseismic deformation.

Based on the above-inferred fault propagation processes, a profile of deformed strata was obtained through forward simulation (Fig. 11a). The predicted profile conformed well to that exposed in the trench. Accordingly, the amounts of fault slip for each boundary since the occurrence of *Earthquake EQ2* are illustrated in Fig. 11b. An accumulated fault slip of 6.45 m was obtained for the pregrowth strata, 6.31 m for the growth strata *Layers h ~ l* (bounded by *Boundaries* #3 and #5), and 4.37 m for the growth strata *Layers a ~ g* (bounded by GL and #3), respectively.

In addition to the current ground surface, the historical ground surfaces before the previous earthquake events were identified as: (1) *Boundary #5* before the *EQ2* event (Fig. 9a); and (2) *Boundary #3* before the *EQ1* event (Fig. 9c). It can be seen that the two ancient ground surfaces are restored to straight lines with very small dip angles, and were almost horizontal (Table 1). The almost horizontal surface implies the layer was either fluvial sediments or lacustrine sediments. Whereas, the restored ground surface before the Chichi event (Fig. 9e) is not a perfect straight line. The fact that the ground surface adopted for inverse analysis was not the actual one but the ground surface of the adjacent trench may account for such phenomenon.

4.2. Comparison with the trench investigation

The historical seismic events can also be revealed by trench investigation. As a result, three events were identified, which are named as *E2*, *E1* and the Chichi event in the sequence of occurrence (Table 2, Chen et al., 2007a).

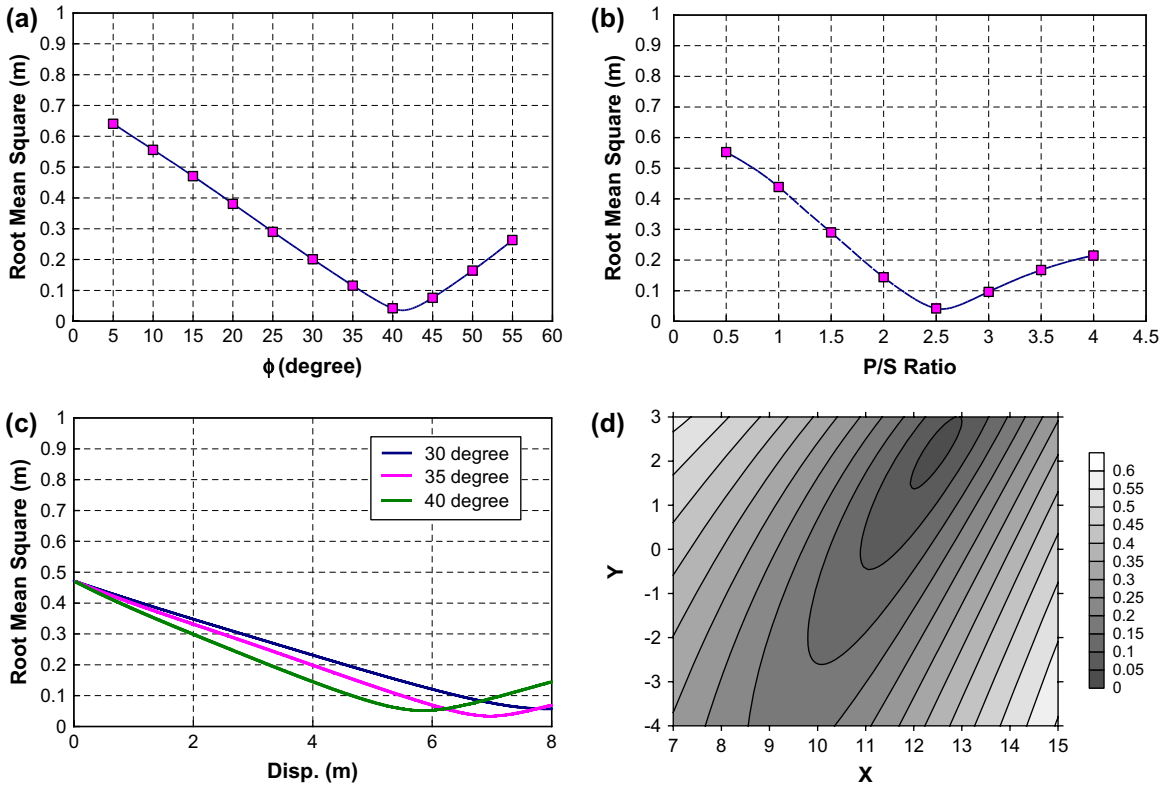

Fig. 8. Slices through root mean square values produced by grid searching over the range of values shown in Fig. 7. The slices show the best fit parameters with least root mean square of error for: (a) trishear angle $2\varphi = 80°$; (b) P/S ratio = 2.5; (c) fault slip = 6.45 m with ramp angle $\theta = 35°$; and (d) the position of fault tip at $x = 12.5$, $y = 2.0$.

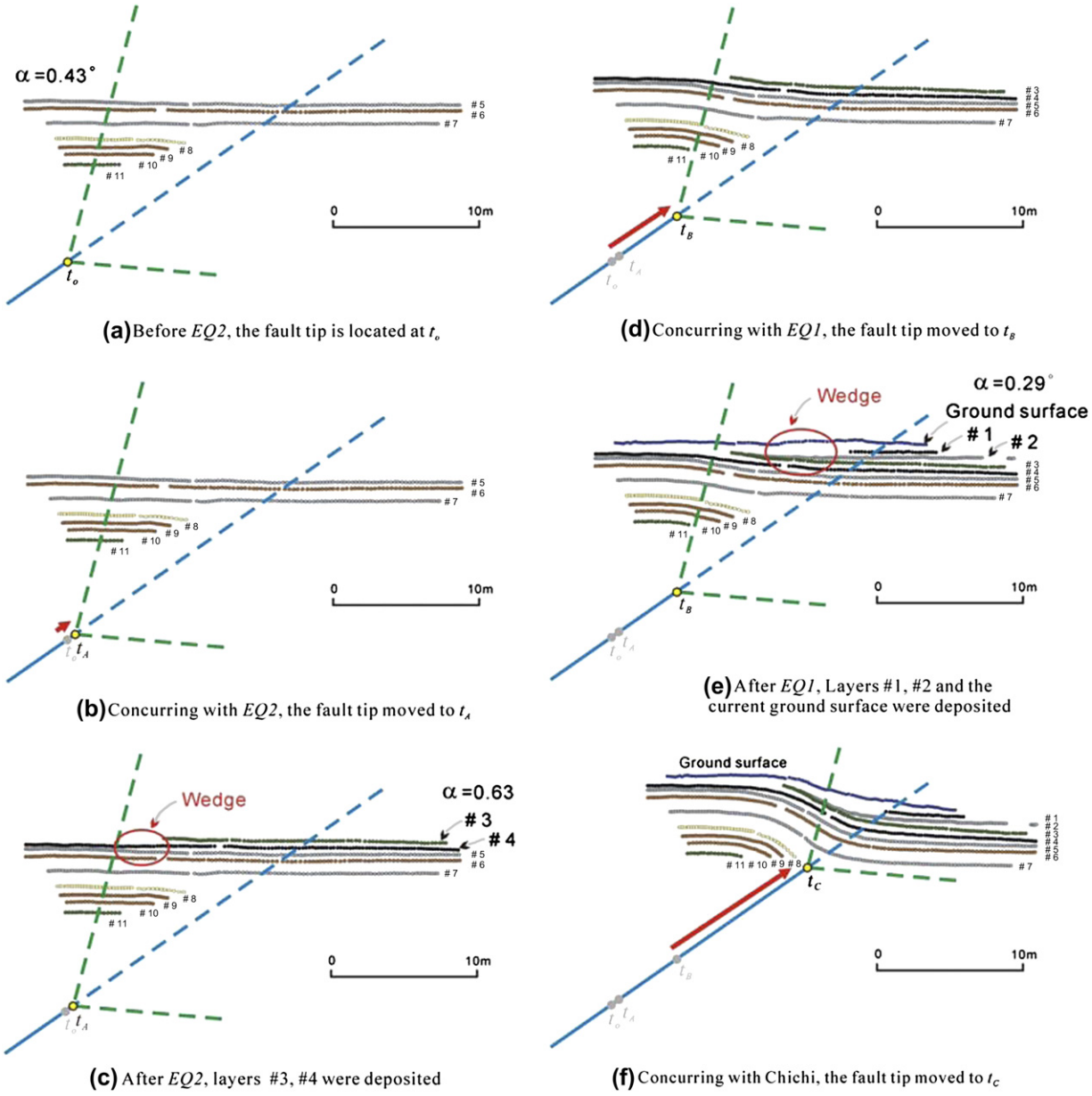

Fig. 9. A forward model with the optimum set of fit trishear parameters showing that the result bears a high likeness to structure exposed in the trench.

Based on mapping of the strata, events identified by the inverse trishear modeling were compared with events identified through trench investigation (Table 2). It can be seen that the deformation induced by the Chichi event and the *E1* event is not distinguished by the inverse trishear analysis. The *E1* event was confirmed by occurrence of a colluvial deposit at the toe of the up-heaved ground. Since in inverse analysis only growth strata were adopted and the existence of the colluvium was neglected, deformations of these two events were not separated and the event *E1* was missed.

Furthermore, the amounts of uplift (S_v) estimated, are 2.51 m for the Chichi event by the inverse trishear analysis; and totaling 1.9 m for the Chichi plus the *E1* events through trench study, respectively. The question as to which is the correct amount then arose. The amount of uplift obtained from the trench study is an estimation based on the deformation of the growth strata inside the trench (Chen et al., 2007a). The range of deformation considered by Chen et al. (2007a) is smaller than that considered in this research through back analysis using trishear model. The elevation difference shown in the trench is only part of the elevation difference and possibly leads to an under-estimation of the uplift; this effect is elaborated in Section 4.4. Ideally, the uplift should be the difference in elevation of the ground surfaces on the hanging wall side and on the footwall side over a sufficiently wide area. When trenching extend failed to cover the highest and/or lowest elevation points, an under-estimation may occur. The coseismic uplift of the Chichi earthquake measured by a nearby GPS station situated 2 km east to the trench is 2.15 m, which is closer to the estimated 2.51 m uplift through

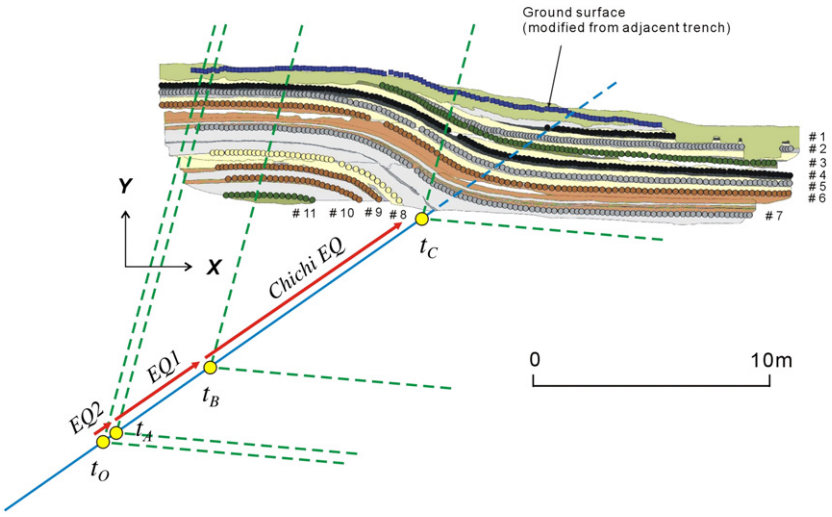

Fig. 10. The locations of fault tips concurred with the three major earthquakes, *Earthquake EQ2*, *EQ1* and the *Chichi EQ* event, respectively. The coordinates of these fault tips are listed in Table 1.

trishear modeling (Fig. 6). Therefore, the actual uplift is possible greater than the one estimated by the trench study. Accordingly, the greater values obtained from the inverse analysis may possibly be more representative. The current uplift of 2.51 m is greater than the 2.15 m far field uplift, the occurrence of a bulge near the fault scarp may possibly account for this small discrepancy (Johnson and Johnson, 2002).

On the other hand, the *EQ2* event was not found by the trench investigation. The *EQ2* was found mainly based on the occurrence of post-*EQ2* onlaps bounded *by Boundaries #3–#5* (Fig. 9). The existence of the onlaps (layers *by Boundaries #3–#5*) in fact point to the existence of a paleoearthquake prior to deposition of these layers. Absence of colluviums exposed below *Boundaries #3* may account for omission of *EQ2* in the trench study. As such, the deformation was considered as the consequence of one event (*E2*), instead of two events (*EQ2* and *EQ1*). Since restoration failed to restore the ground surface and pregrowth strata to straight lines (Fig. 11b), there is reason to consider that the uneven ground was the consequence of yet another preceding event (*EQ2*). Again, the estimated S_v (1.11 m) by the inverse analysis is greater than the S_v (0.7 m) estimated by the trench investigation. Since the layers below *Boundary #8* were not present in the footwall side and only a small portion of them was revealed in the trench, estimation by trench investigation is precluded. On the other hand, the estimation by the inverse analysis accounts for the deformation of the entire extent of layers and assures all layers be restored into straight lines is deemed as reasonable.

4.3. Comparison with the borehole investigation

Strata near surface in most cases comprise soft sediments, and are often disturbed. During borehole drilling they are often lost. In this study core samples lost in drilling operation are marked (Fig. 6). In this case, when the boreholes cored near ground surface, the retrieved cores included a significant amount of missed-cores. It would become difficult, if not impossible, to identify the sedimentary process or perform stratigraphic correlation. Besides revealing the stratigraphic features as well as sedimentary processes, the main purpose of drill holes is to locate the underground fault slip surface. There are two alternatives for the ramp angle of the fault slip surface, 30° and 45°, respectively (Fig. 6).

Trenching investigations along the Chelungpu Fault indicate that the fault slip surface is mainly located at the contact separating the older Pliocene formation (Chinshui Formation, up-thrown block) and the much younger gravel beds (down-thrown block). The dip of this fault slip surface is roughly parallel with the bedding of the Chinshui Formation (e.g. the Pineapple-field site, Chen et al., 2004, 2007a). On the other hand, surficial geological exploration showed that the dip angle of the Chinshui Formation varies from 22° to 39°, which is more consistent with the 30° indicated by the boreholes (Fig. 6). As such, the boundary with a 30° dip angle is more likely the fault slip surface separating Chinshui Formation from the gravel beds (Fig. 6).

Results from boreholes located 3 km southeast of the trench revealed that Toukoshan Formation gravel beds comprising quartzite cobble occurred beneath the Pliocene Chinshui Formation (Fig. 4). Both results from borehole and from shallow seismic reflection survey suggest that the rupture zone activated by the Chichi earthquake coincides with the Chelungpu Fault, with a dip of 38° to the east (Tanaka et al., 2002).

It has been found that, in the observed range of 30° and 38° for ramp angles, when θ equals 35°, all the strata can be restored into gently dipping straight lines. Notably, if θ is greater that 40°, the simulation result indicates that the fault tip should be seen in the trench. However, the fault tip was not observed in the trench; therefore 35° seems to be a reasonable inference for θ (Fig. 6).

4.4. Influence of apical angle

The deformations induced by separate faulting with two different apical angles ($2\varphi = 40°$ and 80°) are chosen to depict

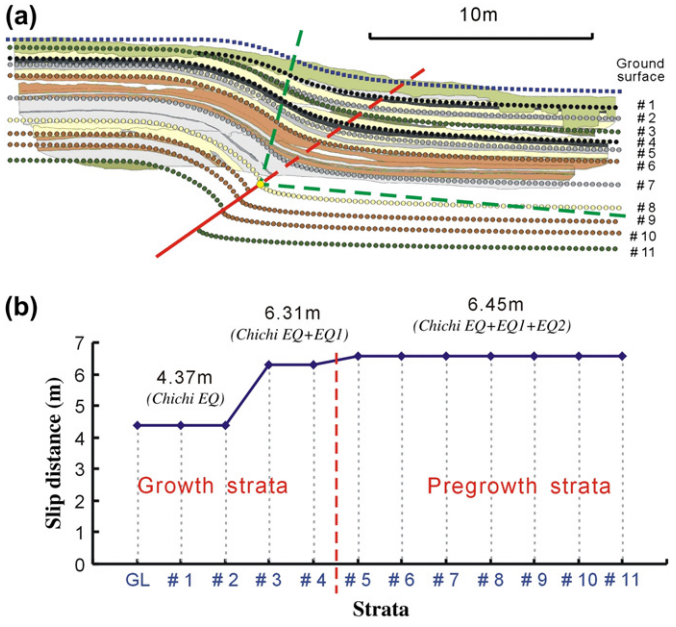

Fig. 11. (a) Comparison of a forward simulation with the growth strata and fold geometry in studied trench. The eleven boundaries match well with the actual layer boundaries. Wedge deposits bounded by *Boundaries # 1* and *#5* and the locations of wedge tips are quite close to the actual ones; (b) The fault slip amount for each stratum boundary since the occurrence of *Earthquake EQ2*. The accumulated fault slips for different layer boundaries are: 6.45 m (*EQ2* + *EQ1* + *Chichi EQ*) for *Boundaries #5* ~ *#11*, 6.31 m (*EQ1* + *Chichi EQ*) for *Boundaries #3* and *#4*, and 4.37 m (*Chichi EQ*) for *Boundaries #1* and *#2*, respectively.

the influence of apical angle (Fig. 12). The fault-propagation fold in the triangular zone above t_f for the former value is much more severely folded than the actual folds revealed by trenching in the studied case (Fig. 12b). On the other hand, configurations of the actual folds in the studied case resemble the ones shown in Fig. 12a. To conform to the actual fold configuration the apical angle would be as high as $(2\theta) = 80°$.

Furthermore, the magnitude of apical angle will also affect the estimated uplift (S_v). During fault propagation the region of deformation is continuously being reduced while the fault tip propagates upward (Fig. 12b). In measuring the amount of uplift (S_v), a smaller S_v will be obtained, if the extent of measurement is not sufficiently long such that it is still within the trishear zone. For the trishear zone with a larger apical angle, the possibility for the actual S_v to be greater than the measured S_v in trench increases. In the studied trench an apical angle as high as 80° may account for the explicitly under-estimating of S_v values through trench study by Chen et al. (2007a).

Table 2
Comparison of coseismic deformation obtained by trench investigation and by this research

Trench investigation (Chen et al., 2007a)		This research	
Event (date)	S_v (m)	Event (date)	S_v (m)
Chichi (1999)	0.8	Chichi (1999)	2.51
E1 (300 ~ 430 BP)	1.1	–	–
E2 (710 ~ 800 BP)	0.7	*EQ1*	1.11
–	–	*EQ2*	0.08

Remarks: Time of the occurrence of the event is estimated from carbon dating.

5. Discussion and conclusion

Revelation of trishear fault-propagation fold characteristics through inverse numerical modeling was proposed by Allmendinger (1998, 2005). This idea was applied in exploring a recently activated fault through an inverse program developed by the authors for this purpose. The results indicated that within the realm of trishear model the methodology seemed appropriate.

The application of the proposed method to actual strata deformed by fault propagation of the Chelungpu Fault in west-central Taiwan unveils the propagation history of the fault. The result showed a fault ramp angle of 35° and the fault underwent at least three movements. Onlap growth strata, deposited following major earthquake events, are appropriately processed during restoration of the folds.

The interpretations of the deformation history obtained by the inverse analysis and trench investigation were then compared. It was found that neither one alone could adequately depict the complete scenario of the coseismic slip history. The combination of these two approaches however seemed to enhance and complement each other and allows a better and more complete understanding of the previous deformation.

The kinematic trishear model relates fold geometry to fault altitude, orientation and displacement. However, controlling factors on fold geometry and triangular shear zones, the influence of soft sedimentary cover on fault propagation and fold development, and whether actual deformation follows the trishear model call for mechanical model (Erickson et al., 2001; Johnson and Johnson, 2002; Cardozo et al., 2003; Cardozo, 2005; Finch et al., 2003, 2004; Hardy and Finch, 2006; Lin et al., 2006). More sophisticated mechanical analyses using the finite and distinct element methods have been conducted, and it was found that the mechanical basis of the trishear modeling is reasonably sound (Cardozo et al., 2003; Finch et al., 2003; Finch et al., 2004; Hardy and Finch, 2006).

Mechanical models, however, also rely on idealized knowledge about the soil and rock behavior, in situ stress, boundary conditions and loading conditions during faulting and folding processes. Besides, it is hard to explicitly model fault tip propagation through mechanical model (Cardozo et al., 2003). Estimation by inverse analysis, on the other hand, accounts for deformation of all of the layers induced by fault movement and allows restoration of every layer into straight lines, and is thus considered as reasonable. For the studied trench, the trishear model enables quantitative estimation of deformations within the overburden sediments and faulting frequency as well as how the fault accumulated slip during previous major earthquakes. This information is useful reference for subsequent hazard assessment purposes (Champion et al., 2001; Lin et al., 2006).

Since the proposed analysis is through the trishear modeling, its correctness depends on whether the trishear model is representative of the actual deformation. Moreover, the

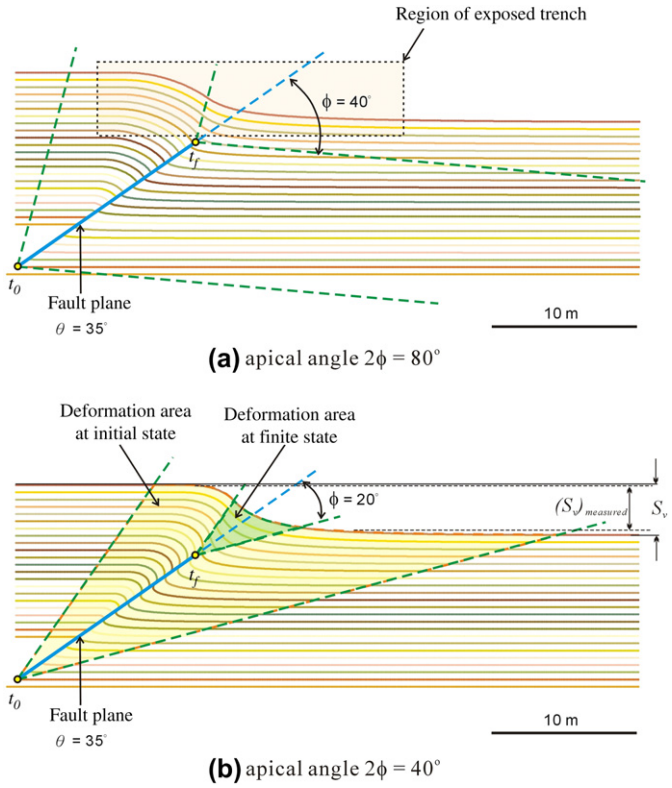

Fig. 12. Influence of apical angle on the triangular shear deformation zones ahead of the fault tips. (a) Apical angle (2φ) = 80°; and (b) Apical angle (2φ) = 40°. The remaining parameters for trishear modeling are the same for both cases: $\theta = 35°$, $P/S = 2.5$, $S = 6$ m, and $H = 10$ m.

proposed trishear model was also based on the assumptions that: (1) the ramp angle of the fault and the *P*/*S* ratio remain constant during all fault propagation events; and (2) the apical angles along both sides of the fault line are equal and would not change for all of the fault propagation events. These assumptions would invariably differ from reality (e.g. the comparison of the results from sandbox and trishear model, Lin et al., 2006), therefore, the inferred fault propagation history would also differ from the actual propagation history. Further evaluation of this discrepancy is necessary.

On the other hand, field observation seems to support, to a certain degree, the inferred trishear deformational process:

(1) the inferred ramp angle during the inverse analysis is about 35°, which is one of the possible ramp angles indicated by nearby boreholes (Fig. 6);
(2) the contact between Chinshui Formation and gravel beds revealed by the boreholes indicates the possible location of the fault surface (Fig. 6). A comparison between Figs. 6 and 10 shows that fault surface revealed by inverse analysis matches well with the contact;
(3) the inferred slip distance triggered by the Chichi earthquake is 4.37 m, which is not far from the slip distance, 3.38 m; measured by GPS station (LM25) located about 2 km from the studied trench (Fig. 4). Meanwhile, the GPS measurement confirms that the slip is coseismic deformation;
(4) last but not least, all of the strata become gently dipping, straight lines after inverse restoration.

In conjunction with the facts that all of the deformed strata can be inverted into straight strata and the inferred deformational process, including the major fault surface are consistent with GPS measurement and borehole logging, the inferred fault propagation history will most likely represent the actual deformation process.

Acknowledgements

The research is partly supported by the National Science Council of Taiwan, grant numbers NSC-90-2211-E-002-095 and NSC-91-2211-E-002-048. The reviewers, Prof. Allmendinger and Cardozo, have kindly provided suggestions that have significantly improved the scientific soundness of this paper. Also, authors thank Mr. Christopher Fong for his help to improve the paper.

References

Allmendinger, R.W., 1998. Inverse and forward numerical modeling of trishear fault-propagation folds. Tectonics 17, 640–656.
Allmendinger, R.W., 2005. www.geo.cornell.edu/geology/faculty/RWA/RWA.html.
Allmendinger, R.W., Shaw, J.H., 2000. Estimation of fault propagation distance from fold shape: implications for earthquake hazard assessment. Geology 28, 1099–1102.
Cardozo, N., 2005. Trishear modeling of fold bedding data along a topographic profile. Journal of Structural Geology 27, 495–502.
Cardozo, N., Bhalla, K., Zehnder, A.T., Allmendinger, R.W., 2003. Mechanical models of fault propagation folds and comparison to the trishear kinematic model. Journal of Structural Geology 25, 1–18.
Central Geological Survey, 2000. Revised Edition of Active Fault Map of Taiwan (1:500,000) and Text. Central Geological Survey, Taipei (in Chinese with English abstract).
Champion, J., Muller, K., Tate, A., Guccione, M., 2001. Geometry, numerical models and revised slip rate for the Reelfoot fault and trishear fault-propagation fold, New Madrid seismic zone. Engineering Geology 62, 31–49.
Chen, W.S., Huang, B.S., Chen, Y.G., Lee, Y.H., Yang, C.N., Lo, C.H., Chang, H.C., Sung, Q.C., Hiang, N.W., Lin, C.C., Sung, S.H., Lee, K.J., 2001a. 1999 Chi-Chi earthquake: a case study on the role of thrust-ramp structures for generating earthquakes. Bulletin of the Seismological Society of America 91, 986–994.
Chen, W.S., Chen, Y.G., Chang, H.C., Lee, Y.H., Lee, K.J., Lee, L.S., Ponti, D.J., Prentice, C., 2001b. Paleoseismology of the Chelungpu Fault, Central Taiwan. 2001 Joint Geosciences Assembly, Taipei, Taiwan, p. 101.
Chen, W.S., Chen, Y.G., Cheng, H.C., 2001c. Paleoseismic study of the Chelungpu fault in the Mingjian area. Western Pacific Earth Sciences 1 (3), 351–358.
Chen, Y.G., Chen, W.S., Lee, J.C., Lee, Y.H., Lee, C.T., Chang, H.C., Lo, C.H., 2001d. Surface rupture of 1999 Chi-Chi earthquake yields insights on active tectonics of central Taiwan. Bulletin of the Seismological Society of America 91, 977–985.
Chen, W.S., Lee, K.J., Lee, L.S., Ponti, D.J., Prentice, C., Chen, Y.G., Chang, H.C., Lee, Y.H., 2004. Slip rate and recurrence interval of the Chelungpu fault during the past 1900 years. Quaternary International 115-116, 167–176.
Chen, W.S., Lee, K.J., Lee, L.S., Streig, A.R., Chang, H.C., Lin, C.W., 2007a. Paleoseismic evidence for coseismic growth-fold in the 1999 Chichi earthquake and earlier earthquakes, central Taiwan. Journal of Asian Earth Sciences. doi:10.1016/j.jseaes.2006.07.027.

Chen, W.S., Yang, C.C., Yen, Y.C., Lee, L.S., Lee, K.J., Yang, H.C., Chang, H.C., Ota, Y., Lin, C.W., Lin, W.H., Shih, T.S., Lu, S.T., 2007b. Late holocene paleoseismicity of the southern portion of the Chelungpu Fault, Central Taiwan: Evidence from the Chushan excavation site. Bulletin of the Seismological Society of America 97 (1), 1–13.

Cristallini, E.O., Allmendinger, R.W., 2001. Pseudo 3-D modeling of trishear fault-propagation folding. Journal of Structural Geology 23, 1883–1899.

Erickson, S.G., Strayer, L.M., Suppe, J., 2001. Initiation and reactivation of faults during movement over a thrust-fault ramp: numerical mechanical models. Journal of Structural Geology 23, 11–23.

Erslev, E.A., 1991. Trishear fault-propagation folding. Geology 19, 617–620.

Finch, E., Hardy, S., Gawthorpe, R.L., 2003. Discrete element modeling of contractional fault-propagation folding above rigid basement fault blocks. Journal of Structural Geology 25, 515–528.

Finch, E., Hardy, S., Gawthorpe, R.L., 2004. Discrete element modeling of extensional fault-propagation folding above rigid basement fault blocks. Basin Research 16, 489–506.

Ford, M., Williams, E.A., Artoni, A., Vergés, J., Hardy, S., 1997. Progressive evolution of a fault propagation fold pair as recorded by growth strata geometries, Sant Llorenç de Morunys, SE Pyrenees. Journal of Structural Geology 19, 413–441.

Hardy, S., Finch, E., 2006. Discrete element modelling of the influence of cover strength on basement-involved fault-propagation folding. Tectonophysics 415, 225–238.

Hardy, S., Ford, M., 1997. Numerical modeling of trishear fault propagation folding. Tectonics 16, 841–854.

Hardy, S., McClay, K., 1999. Kinematic modeling of extensional fault-propagation folding. Journal of Structural Geology 21, 695–702.

Hung, J.H., Wiltschko, D.V., 1993. Structure and kinematics of arcuate thrust faults in the Miaoli-Cholan area of western Taiwan. Petroleum Geology of Taiwan 28, 59–96.

Johnson, K.M., Johnson, A.M., 2002. Mechanical models of trishear-like folds. Journal of Structural Geology 24, 277–287.

Lee, J.C., Chen, Y.G., Sieh, K., Mueller, K., Chen, W.S., Chu, H.T., Chan, Y.C., Rubin, C., Yeats, R., 2001. A vertical exposure of the 1999 surface rupture of the Chelungpu fault at Wufeng, western Taiwan: structural and paleoseismic implications for an active thrust fault. Bulletin Seismological of America 91 (5), 914–929.

Lee, J.C., Rubin, M.C., Mueller, K., Chen, Y.G., Chan, Y.C., Sieh, K., Chu, H.T., Chen, W.S., 2004. Quantitative analysis of movement along an earthquake thrust scarp: a case study of a vertical exposure of the 1999 surface rupture of the Chelungpu fault at Wufeng, western Taiwan. Journal of Asian Earthquake Science 23, 263–273.

Lin, M.L., Chung, C.F., Jeng, F.S., 2006. Deformation of overburden soil induced by thrust fault slip. Engineering Geology 88, 70–89.

Ota, Y., Huang, C.Y., Yuan, P.B., Sugiyama, Y., Lee, Y., Watanabe, M., Sawa, H., Yanagida, M., Sasake, S., Tanifuchi, K., 2001. Trenching study at the Tsaotun site in the central part of the Chelungpu Fault, Taiwan. Western Pacific Earth Sciences 1 (4), 487–498.

Ota, Y., Chen, Y.G., Chen, W.S., 2005. Review on paleoseismological and active fault studies in Taiwan in the light of the Chichi earthquake of September 21, 1999. Tectonophysics 408, 63–77.

Suppe, J., Medwedeff, D.A., 1990. Geometry and kinematics of fault-propagation folding. Eclogae Geologicae Helvetiae 83, 409–454.

Tanaka, H., Wang, C.Y., Chen, W.M., Sakaguchi, A., Ujiie, K., Ito, H., Ando, M., 2002. Initial science report of shallow drilling penetrating into the Chelungpu fault zone. Taiwan. TAO 13 (3), 227–251.

Withjack, M.O., Olson, J., Peterson, E., 1990. Experimental models of extensional forced folds. American Association of Petroleum Geologists Bulletin 74, 1038–1045.

Zehnder, A.T., Allmendinger, R.W., 2000. Velocity field for the trishear model. Journal of Structural Geology 22, 1009–1014.